Proceedings of the 21st ICSMGE, Vienna, Austria, 14 – 19 June 2026. Pistrol, Adam & Schweiger (eds.)
Published by: ÖGG, Austrian Society for Geomechanics, Salzburg, Austria, ISBN 978-3-9503898-4-5
https://doi.org/10.53243/ICSMGE2026-446

Deformation and fracture studies in confined indentation of porous rock-like materials

Peerzadi Arzeena Imtiyaz, **Shwetabh Yadav**
Department of Civil Engineering, Indian Institute of Technology Hyderabad, Hyderabad, India, shwetabh@ce.iith.ac.in

ABSTRACT: This study investigates the mechanics of deformation of rocks experimentally. Gypsum was used as a model material, allowing control over sample geometry and porosity. Wedge indentation experiments were performed under plane strain conditions. Samples were confined in the directions perpendicular to the motion of indenter to replicate field conditions encountered in geotechnical and mining applications. In situ images of the region surrounding the indenter were captured to obtain the development of deformation zone followed by initiation and propagation of fracture at its boundary. Captured images were analyzed to obtain full field deformation parameters such as displacement, strain rate and fracture morphology. The analysis revealed a transition from ductile (observable deformation zone) to brittle (propagation of tensile cracks) failure as a function of confining stress. It was observed that higher confinement not only suppresses early fracture but also requires greater force for continued penetration. With implications for improving tool design and operational parameters in drilling and excavation procedures to limit fracture and deformation, these findings provide insights on the micromechanical behavior of porous rock-like materials under confined indentation.

KEYWORDS: Confined indentation, fracture studies, high-speed imaging, PIV.

1 INTRODUCTION

Indentation tests have long been used to evaluate rock fracture and deformation mechanisms under localized tool loading. Foundational laboratory studies employing two-dimensional wedge indenters, functionally similar to single cutting tools, helped reveal primary failure modes and controlling factors. For instance, Chen & Labuz (2006) conducted servo-hydraulic wedge indentation on dry rocks, carefully monitoring displacement using speckle interferometry and acoustic emission. Their results demonstrated that rock strength parameters, indenter geometry (particularly wedge angle), and the degree of lateral confinement fundamentally govern failure. They also reported the formation of a compacted (plastic) zone beneath the indenter and the nucleation of tensile cracks at the interface between plastic and elastic zones. Extending these insights, Saadati et al. (2020) performed 3D indentation experiments on intact sandstone blocks, illustrating contrasting fragmentation behaviors in rocks of varying strength. Strong rocks (like granite or diabase) exhibited a pronounced force peak, catastrophic failure, and fragment ejection, whereas weaker and more porous rocks (such as sandstone and limestone) showed significant plastic flow with minimal fragmentation.

Confinement conditions further influence cracking and deformation patterns. While most historical indentation tests involved unconfined or weakly confined loading, studies show that lateral or confining stresses dramatically change crack initiation sites and fragment patterns. Notably, numerical modeling by Huang et al. (1998) predicted that even small confining pressures cause the peak tensile stress region to move away from the indenter axis and induce more horizontal, deeper-initiated cracks. This means that as lateral stress increases, subsurface cracks form deeper and at steeper angles, even though the overall maximum tensile stress and required indentation load change minimally. Chen & Labuz (2006) also observed experimentally that higher confinement shifts wedge indentation failure from brittle splitting towards more ductile, plastic flow.

Advancements in real-time in situ imaging have more recently refined understanding of indentation-induced failure. Yadav et al. (2016), using plane-strain wedge indentation with particle-image velocimetry (PIV) on porous rocks like gypsum, directly tracked deformation fields during loading. They found that highly porous specimens responded with more ductile flow and no abrupt cracking, whereas low-porosity samples fractured suddenly under comparable conditions. High porosity correlated with increased ductility and compaction prior to any visible crack. Similarly, Zhang et al. (2012) used digital image correlation while indenting sandstone and observed that localized shear bands and slip zones precede the dominant splitting fracture mode, confirming the general sequence where plastic compaction and distributed sliding localize into discrete cracks when stress concentrates.

Although these studies deepen the understanding of indentation processes, the precise effects of lateral confinement on fracture and deformation remain inadequately addressed, especially in the absence of real-time high-resolution observation. Traditional load–displacement data, while informative, do not capture the intricacies of dynamic failure under confined conditions. The present study addresses this gap by combining precisely controlled lateral confinement with in situ optical imaging. Indentation experiments are performed on porous gypsum at two confinement levels (0.5kN and 6kN), while high-speed imaging tracks evolving deformation and velocity fields. This approach enables the direct visualization of brittle-to-ductile transitions in response to confinement, providing new insights into how lateral stress controls the mechanical response of porous rocks.

2 METHODOLOGY

2.1 *Sample preparation*

In this study, gypsum was chosen as a representative material to model the mechanical behavior of brittle rocks under indentation (Vekinis et al. 1993; Bobet & Einstein 1998; Yadav et al. 2015). The test samples were prepared using calcium sulphate hemihydrate ($CaSO_4 \cdot ½H_2O$), commonly known as Plaster of Paris (POP). Mixing the hemihydrate powder with distilled water initiates a hydration reaction, resulting in the formation of gypsum ($CaSO_4 \cdot 2H_2O$) which sets into a solid matrix suitable for mechanical testing.

For sample preparation, a freshly mixed slurry of POP was poured into cubic molds with dimensions of 150mm × 150mm × 150mm. During casting, a sheet of sandpaper was placed at the bottom of the mold to impart a textured surface on one face of each sample. This textured surface introduced asperities that facilitated speckle generation for subsequent Particle Image Velocimetry (PIV) analysis. After casting, the samples were demolded and left to cure under ambient laboratory conditions (approximately 25 ± 2 °C) for 48 hours and then oven-dried at

45°C for additional 48 hours to ensure full setting and moisture stabilization before testing. The main physical and mechanical properties of the prepared gypsum samples are given in Table 1.

Table 1. This is a table caption.

Parameter	Symbol	Value	Unit
Porosity	n	50	%
Static compressive strength	σ_c	11	MPa
Young's modulus	E	3	GPa

2.2 *Test set-up*

The experimental setup employed in this study was designed to facilitate wedge indentation testing under controlled lateral confinement. A custom-built indentation-die assembly (see Figure 1) was used, incorporating provisions for the application of biaxial confining pressure through two hydraulic cylinders acting on two perpendicular faces of the sample. The gypsum sample was securely placed within the sample holder. A wedge indenter with an included angle of 120° was used to apply the vertical load on the sample surface. The indentation load was delivered using a servo-controlled actuator with a maximum capacity of 100 kN, operated at a constant loading rate of 0.5 mm/min. The outer confining box included a transparent observation window to enable real-time deformation monitoring through imaging. To capture the deformation and fracture processes, high-speed image acquisition was carried out using a Phantom VEO 310L camera at a frame rate of 24 frames per second (fps). Two levels of lateral confinement were examined: Case a with 0.5 kN and Case b with 6 kN, applied via the hydraulic cylinders. This allowed for a systematic investigation of the influence of confinement on the deformation behavior and fracture mechanisms under indentation.

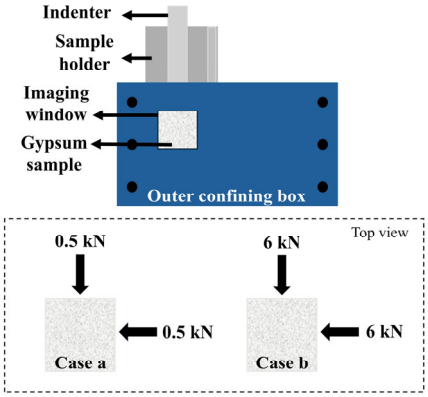

Figure 1. Schematic diagram of confined indentation-die setup.

3 RESULTS AND DISCUSSION

3.1 *Indentation under lower confinement (0.5 kN)*

Figure 2 and Figure 3 show the full-field results obtained from the in-situ image analysis for the indentation of a gypsum sample under a low lateral confining load of 0.5 kN. Specifically, Figure 2 illustrates the velocity field (v in mm/s) while Figure 3 presents the corresponding effective strain rate field ($\dot{\epsilon}$ in s^{-1}) under the same loading condition. These maps are captured using high-speed imaging at 24 fps during wedge indentation with a 120° indenter. For each figure, four frames i.e., Frame 1 (153 s), Frame 2 (249 s), Frame 3 (287 s), and Frame 4 (728 s) are presented to depict the temporal evolution of the deformation process.

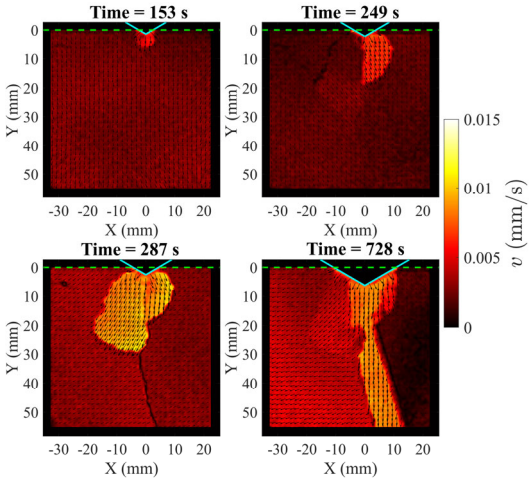

Figure 2. Velocity field map for indentation of gypsum sample with 120° indenter at 0.5 kN confining load.

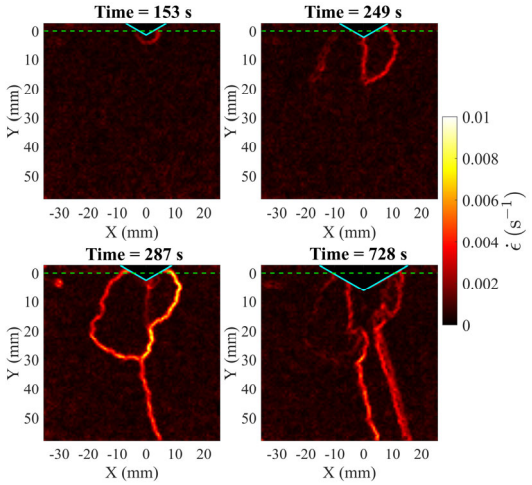

Figure 3. Effective strain rate field map for indentation of gypsum sample with 120° indenter at 0.5 kN confining load.

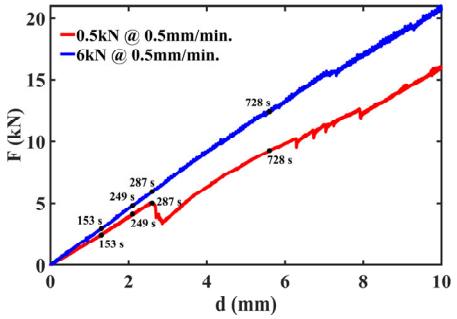

Figure 4. Force penetration curves for indentation of gypsum sample with 120° indenter at varying confining loads of 0.5 kN and 6 kN.s

In the 0.5 kN test (Figure 2), the velocity maps reveal a concentrated deformation zone just beneath the indenter, bordered by essentially stationary material. By Frame 3, a sharp tensile crack emerges from the indenter tip downward. This sequence – first a crushed (compacted) zone under the indenter and then a crack initiating at a critical depth – is exactly what one expects for brittle rock indentation. In fact, past studies of wedge indentation in porous gypsum show that the region near the indenter moves with almost the full indentation velocity while the far-field remains still, matching our observations (Yadav et al. 2016). The effective strain-rate field (Figure 3) similarly shows a strong localization of strain right where the crack forms. Crucially, the crack appears at the same depth

where the load–penetration ($F-d$) curve (Figure 4) exhibits a sudden drop (Frame 3). Such sawtooth drops are a well-known signature of brittle fracture: each load peak corresponds to stress buildup and the drop to crack propagation (Yagiz 2009). Thus, under low confinement the gypsum behaves in a classic brittle manner – a large elastic/plastic zone forms first, then tensile failure occurs once stresses exceed the rock's fracture threshold.

3.2 *Indentation under higher confinement (6 kN)*

Similar to Figure 2 and Figure 3, Figure 5 and Figure 6 show the full-field results obtained from the in-situ optical analysis for the indentation of a gypsum sample under a higher lateral confining load of 6 kN. These maps are also captured using high-speed imaging at 24 fps during wedge indentation with a 120° indenter. As in the earlier figures, four frames correspond to time intervals of 153 s (Frame 1), 249 s (Frame 2), 287 s (Frame 3), and 728 s (Frame 4) are presented to depict the temporal evolution of the deformation process. In addition, Figure 7 provides a composite map of both velocity (v in mm/s) and strain rate ($\dot{\epsilon}$ in s^{-1}) fields to highlight localized deformation zones and crack evolution under elevated confinement.

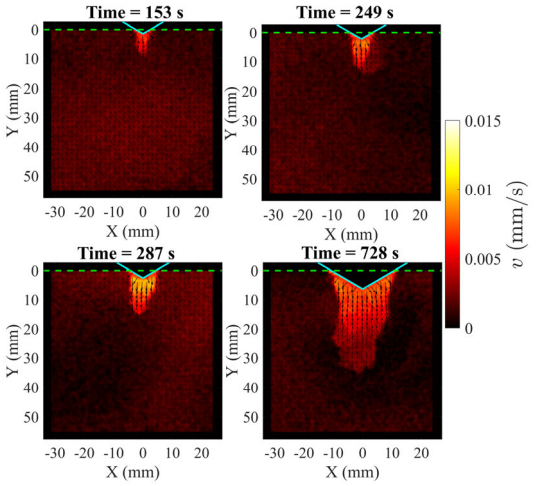

Figure 5. Velocity field map for indentation of gypsum sample with 120° indenter at 6 kN confining load.

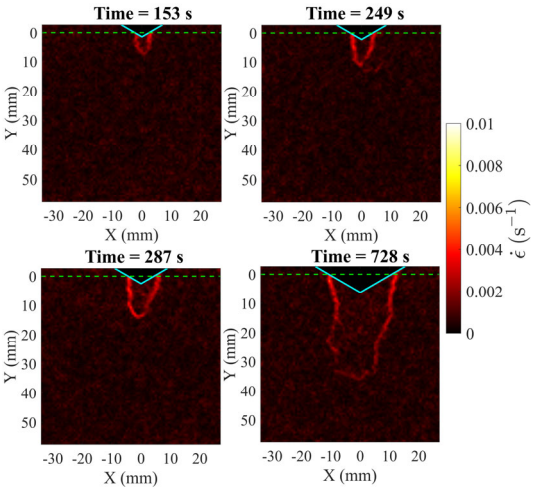

Figure 6. Effective strain rate field map for indentation of gypsum sample with 120° indenter at 6 kN confining load.

In contrast, at 6 kN confining pressure (Figure 5) the sample shows a much larger deformation zone with no cracks till Frame 4. The strong lateral compression evidently raises the stress needed for fracturing. In the velocity and strain maps (Figure 6), deformation remains broadly distributed under the indenter with no high-strain focal point, indicating that the rock is compacting rather than cracking. This behavior resembles a ductile compaction response rather than brittle failure. Accordingly, the load–penetration curve (Figure 4) is smooth and nearly linear, with none of the drops seen in the higher confinement case. This difference confirms that higher confinement not only suppresses early cracking but also requires significantly greater force for continued penetration, as is visually evident in Figure 4.

Figure 7 shows the velocity and effective strain rate field during indentation of the gypsum sample with a 120° indenter under 6 kN confining load, along with actual image of sample taken during the experiment. These images depict the localized deformation zone and eventual crack formation. A notable observation from this figure is that a tensile crack forms only at a much later stage, specifically at 977 s, initiating at the boundary of the deformation zone. This delayed fracture behavior under confinement agrees with numerical predictions by Huang et al. (1998) who stated that even modest confining pressure shifts the peak tensile stress laterally and delays crack initiation. In other words, confinement does not eliminate the tensile stresses (which still eventually break the rock) but it prevents them from opening a visible surface crack until very large indentation. Further studies exploring crack initiation and propagation under increased confinement using in situ measurement techniques are currently in progress.

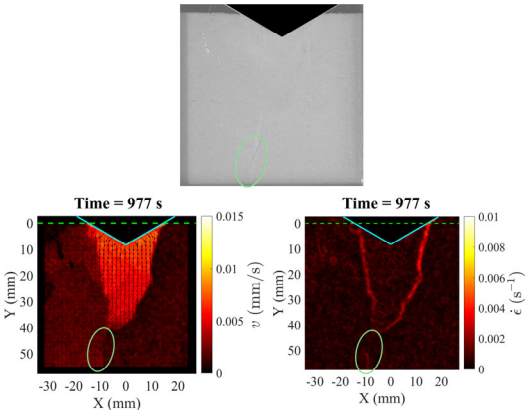

Figure 7. Velocity and effective strain rate field map for indentation of gypsum sample with 120° indenter at 6 kN confining load, along with actual image of sample taken during experiment.

4 CONCLUSIONS

This study investigated the deformation and fracture response of gypsum under varying levels of lateral confinement using wedge indentation combined with in-situ measurement techniques. The results reveal how confinement governs the transition from brittle to ductile-like behavior in indentation processes. By comparing velocity and strain rate fields at low and high confining loads, along with corresponding force–penetration trends, several key insights emerge regarding failure mechanisms, crack initiation, and load resistance:

- Under 0.5 kN confining pressure the gypsum developed a pronounced crushed (deformation) zone under the indenter and then failed by tensile cracking at a critical penetration (Frame 3). This sequence – a ductile-like compaction zone followed by a sudden crack – matches classical brittle indentation behavior.
- Applying 6 kN lateral stress dramatically delayed fracture. No crack was seen even at deep penetration (Frame 4); instead, the rock deformed broadly under the indenter. This

is consistent with the theory that confinement shifts the tensile failure point laterally and inhibits opening of new cracks.

- The unconfined test shows multiple load drops in its force–penetration curve (sawtooth pattern) coinciding with crack events, as expected for brittle failure. The confined test, by contrast, yields a smooth curve with higher overall load, indicating continuous compaction. In summary, force drops mark crack formation in brittle rock, whereas smooth loading implies no fracture.
- The confined sample carried much greater load at large penetration, reflecting the well-known effect that lateral pressure raises rock strength. Lateral stress therefore not only delays cracking but also increases the rock's load-bearing capacity.

5 ACKNOWLEDGEMENTS

The authors sincerely acknowledge IIT Hyderabad for providing the research facilities and institutional support essential for this work. This study was supported through a seed grant (No. SG-104) from IIT Hyderabad.

6 REFERENCES

Bobet, A., and Einstein, H. H. 1998. Fracture coalescence in rock-type materials under uniaxial and biaxial compression. *International Journal of Rock Mechanics and Mining Sciences* 35, 863-888.

Chen, L. H., and Labuz, J. F. 2006. Indentation of rock by weddge-shaped tools. *International Journal of Rock Mechanics and Mining Sciences* 43, 1023-1033.

Huang, H., Damjanac, B., and Detournay, E. 1998. Normal Wedge Indentation in Rocks with Lateral Confinement. *Rock Mechnaics and Rock Engineering* 31, 81-94.

Saadati, M., Weddfelt, K., and Larsson, P. L. 2020. A Spherical Indentation Study on the Mechanical Response of Selected Rocks in the Range from Very Hard to Soft with Particular Interest to Drilling Application. *Rock Mechanics and Rock Engineering* 53, 5809-5821.

Vekinis, G., Ashby, M. F., and Beaumont, P. W. R. 1993. Plater of paris as a model material for brittle porous solids. *Journal of Materials Science* 28, 3221-3227.

Yadav, S., Saldana C., and Murthy, T. G. 2015. Deformation field evolution in indentation of a porous brittle solid. *International Journal of Solids and Structures* 66, 35-45.

Yadav, S., Saldana, C., and Murthy, T. G. 2016. Porosity and geometry control ductile to brittle deformation in indentation of porous solids. *International Journal of Solids and Structures* 88-89, 11-16.

Yagiz, S., and Rostami, J. 2009. Using indentation test to compute rock brittleness index. *Proc. 46th US Rock Mechanics / Geomechanics Symposium,* Chicago, IL, USA, 24-27 June.

Zhang, H., Huang, G., Song, H., and Kang, Y. 2012. Experimental investigation of deformation and failure mechanisms in rock under indentation by digital image correlation. *Engineering Fracture Mechanics* 96, 667-675.